Nonlinear Self-Accelerating Optical Fields and Their Applications

Jia Peng-Bo, Pei Yu-Miao, Zhang Ping, Li Zhi-Li, Hu Yi *, Xu Jing-Jun

The MOE Key Laboratory of Weak-Light Nonlinear Photonics,
TEDA Applied Physics Institute and School of Physics, Nankai University, Tianjin 300457, China

Abstract: Optical Airy beams or pulses, famous for a self-accelerating intense peak, have recently attracted a great deal of attention triggered by their intriguing properties and unique advantages in a variety of applications. Under the action of nonlinearities, such wave packets tend to lose their peculiar structures and the associated accelerating dynamics are accordingly degraded. To circumvent this inconvenience, nonlinear self-accelerating beams/pulses were conceived, leading to more possibilities to shape a nonlinear process into an accelerating configuration. Here, we present a review on these nonlinear self-accelerating wave packets following our recent works. Their physical picture and connection with the Airy wave packets are discussed. Then we focus on their accelerating property that shows exotic features in controlling nonlinear dynamics, visualizing optical nonlinear responses and guiding other light. In the end, a new kind of self-accelerating beams is introduced, exhibiting a mechanism in analogy to the interaction between matters of opposite mass signs. These nonlinear wave packets have brought the nonlinear dynamics into a region of a curved space or space-time, and more fantastic phenomena and applications which are otherwise hard to reach in flat space are expected.

Key words: Optical field manipulation; Optical nonlinear dynamics; Optical Airy field; Self-acceleration

CLC number: O437 **Document Code:** A **DOI:** 10.13725/j.cnki.pip.2020.05.002

CONTENTS

Received date: 2020-9-10
*Email: yihu@nankai.edu.cn

I. INTRODUCTION

Inspired by the concept of self-acceleration [1] for a wave packet found in the potential-free Schrödinger equation, a laser light shaped by an Airy function was conceived, namely Airy beam [2,3], featured with an intense peak moving along a ballistic path during the free space propagation. In the same vein (due to a space-time duality), an optical pulse with an Airy shape exhibits an accelerating behavior in a dispersive medium. Soon after, this kind of optical fields attracted a great deal of attention. The exotic property of self-acceleration, together with the accompanying less diffraction/dispersion and self-healing effect, led the Airy beam/pulse to show unexpected advantages in a variety of applications such as in optical manipulation [4,5], imaging [6−8], material processing [9], signal transmis-

sion [10−12] and optical bullet [13,14]. In turn, these promising applications promoted more extensive studies on the design and generation of other types of accelerating beams and their ramifications (see the reviews in [15−17] and the references within).

Apart from the intensive studies in the linear regime, numerous investigations on the nonlinear dynamics of optical Airy wave packets were carried on in parallel. In the spatial domain, Airy beams were employed to produce curved filamentation [18−20] and were widely examined in various nonlinear environments offered by different types of nonlinearities, such as Kerr, saturable, quadratic, and nonlocal nonlinearity [21−31]. In the temporal domain, the Airy pulses were mostly explored in nonlinear optical fibers [32−45]. Novel applications were put forward in terms of wavelength conversion and pulse control [46,47]. Besides, the nonlinear dynamics of Airy-pulse related novel fields were also studied [13,48]. Indeed, the Airy wave packets are the eigenmodes of a linear system (i.e., described by a Schrödinger-like equation). Consequently, as shown in most studies, they tend to lose their peculiar structures under the action of the nonlinearity and cease to accelerate, for instance, by transforming most of their power into other nonlinear entities such as solitons. To keep the acceleration, one need resort to the solutions satisfying the nonlinear Schrödinger-like equation. With this motivation, nonlinear accelerating wave packets were created fitting to various types of nonlinearities. Thanks to these findings, the properties of self-acceleration can be largely explored in nonlinear environments, allowing for more novel phenomena and effects by shaping a nonlinear process in an accelerating configuration.

In this short review, we discuss the nonlinear accelerating optical fields and the applications they brought about, by focusing more on our recent works pertinent to this area. The organization of the review is as follows: In Section II, a theoretical basis is provided to highlight the physical picture of the nonlinear accelerating waves; in Section III, we show unexpected nonlinear phenomena and effects associated with the acceleration, focusing on the visualization of a nonlinear response; in Section IV, we discuss the light-by-light control realized by nonlinear accelerating beams/pulses; in Section V, a new kind of self-accelerating state is introduced, exhibiting a mechanism in analogy to the interaction between matters having opposite mass signs; in Section VI, we conclude the review and give an outlook on the nonlinear accelerating optical fields.

II. THEORY ON NONLINEAR ACCELERATING WAVE PACKETS

Considering the law of momentum conservation, people earlier believed that nonlinear self-trapped beams with acceleration could only exist in asymmetric nonlinearities. Such states were found for the first time in photorefractive medium owned to a small asymmetric contribution from the diffusion effect [22]. But later on, optical self-accelerating self-trapped beams were also proposed in symmetric nonlinearities including Kerr, saturable types, etc [49−52]. In the following, we will briefly introduce the associated theoretical findings and their connection with the Airy solutions.

In general, the nonlinear optical dynamics can be simply described by the nonlinear Schrödinger equation. With different types of nonlinearities, this equation has a generalized form, namely the generalized nonlinear Schrödinger equation:

$$\frac{\partial\psi}{\partial\zeta} = \frac{i}{2}\frac{\partial^2\psi}{\partial\xi^2} - if(I)\psi \tag{1}$$

where ψ represents a wave packet, ξ indicates the normalized temporal or spatial transverse coordinate, and ζ is the normalized propagation distance. $f(I)$ is a real-valued algebraic function representing different types of nonlinearities and $I = |\psi|^2$ is the wave intensity. It is possible to transform the original coordinates into an accelerating frame by using $s = \xi - h\zeta^2/2$ (h is a constant), and $\psi = u(s)\exp(ih^2\zeta^3/6 + ih\zeta\xi)$ (where u is a real-valued function), Eq.(1) is then rewritten as in a steady state:

$$\frac{\mathrm{d}^2u}{\mathrm{d}s^2} - 2hsu - 2f(I)u = 0 \tag{2}$$

Obviously, a gravity-like potential is introduced in this accelerating system. Without loss of generality, h is set to be positive. Under the linear condition (i.e., $f(I) = 0$), an Airy solution exists, consisting of a main lobe and infinite sub-lobes towards the left [Fig.

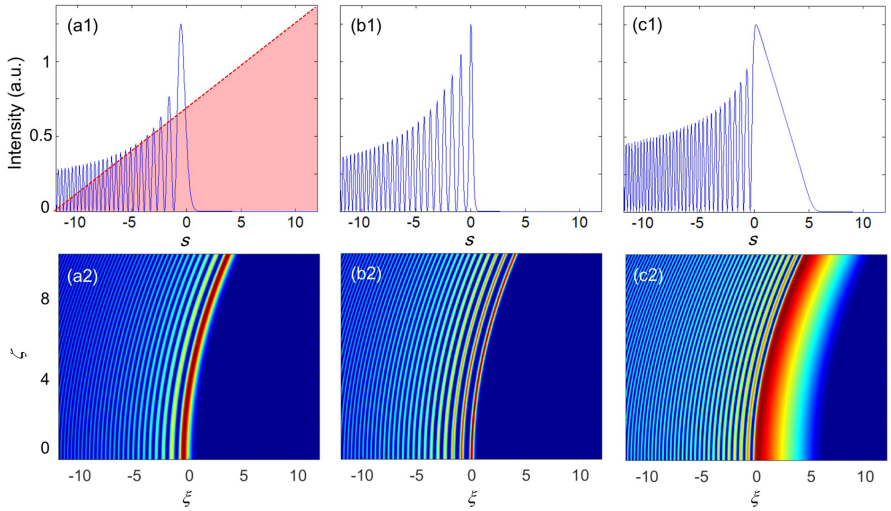

FIG. 1. Self-accelerating optical fields in linear and nonlinear environments. Top and bottom rows present the typical intensity profiles and the associated propagations, respectively. From left to right correspond to the linear, weak self-focusing and self-defocusing cases. The red shaded area in (a1) shows the gravity-like potential introduced in the accelerating frame.

1(a1)]. One can attribute the semi-infinite profile to the fact that only the right side of a wave experiences an infinite potential barrier [Fig. 1(a1)]. An optical beam reshaped as the Airy function can keep the transverse acceleration and diffraction-free propagation in the laboratory coordinate [Fig. 1(a2)]. Then we turn to the nonlinear regime ($f(I) \neq 0$). As a typical example, the Kerr nonlinearity (i.e., $f(I) = n_2 I$, where n_2 is the nonlinear coefficient) is considered. Nonlinear self-accelerating beams are obtained numerically. Since the nonlinearly induced potential does not alter the infinite nature of the barrier considering the intensity limit of waves, these modes have structures similar to the Airy case, but in comparison, their main lobes exhibit shrinking and broadening changes under the self-focusing and -defocusing nonlinearities, respectively [Figs. 1(b1) and 1(c1)]. Like the self-accelerating behavior of the Airy wave packets, these nonlinear self-accelerating beams propagate stably along the same parabolic trajectory in the associated nonlinear environments. However, under a strong self-focusing condition, the nonlinear states are unstable, and the intense lobes of the beam tend to form solitons emitting in various directions [49].

The method to solve the nonlinear self-accelerating modes was extended into other optical systems where the nonlinearity is not simply described by a real-valued algebraic function. In quadratic media, the first and second harmonics show a propagation of a joint acceleration, but their intensity peaks are asynchronous with respect to each other [24,25]. Under a highly nonlocal nonlinearity, self-accelerating nonlinear modes exist by reducing the associated nonlinear system into a linear model called Snyder – Mitchell model [53]. With the help of nonlocality, the stationary accelerating propagation of two dimensional (2D) Airy beams in strong self-focusing medium can be obtained [29]. Besides, nonlinear counterparts of non-paraxial accelerating beams [54,55], an extension of the Airy case into the non-paraxial condition, were also realized [56–58]. Apart from the continuous cases, accelerating Wannier-Stark states were also demonstrated in discrete photonic lattices [59,60].

III. ACCELERATING NONLINEAR PROCESSES

Under a mild nonlinearity, an Airy wave packet can still keep the acceleration. When the nonlinear strength is sufficiently large, both theory and experiment have indicated that this optical field deforms inevitably and fails to accelerate in a shape-preserving form [21,23]. In particular, the phenomenon of soliton emission appears in a strong self-focusing regime. Such dynamics have

been investigated in both Kerr and photorefractive media [61–63].

Fortunately, recent work has demonstrated that, during the propagation, a modulated Airy wave packet can avoid the deformation and keep the acceleration under an adiabatic condition [51]. Similar to the evolution from a Gaussian beam into a soliton, the modulated Airy field tends to evolve into the nonlinear self-accelerating wave packet. Along this line, nonlinear accelerating beams/pulses with an intense peak intensity become realistic, which is beneficial to study novel nonlinear phenomena caused by the acceleration.

Resorting to the nonlinear self-accelerating optical fields, nonlinearly induced dipole can be generated to move in an accelerating configuration, probably reshaping its radiation. For instance, we consider the optical Cherenkov radiation in fibers [44], where the light-induced dipole radiates dispersive waves (DWs) under the action of higher order dispersions. For an input pulse shaped as a fundamental soliton, it emits a DW that is similar to a plane wave radiation, as the solition moves at a constant velocity. By means of a modulated Airy pulse, the resulting DW converges at a spatiotemporal location. Such DW focusing dynamics can be further controlled by changing the parameters of the pulse. Via turning up the input power or decreasing the phase modulation depth, the acceleration of the pulses tends to increase, thus leading to a stronger DW focusing. These results pave a way to control the radiation by means of nonlinear accelerating pulses. Quite recently, such kind of optical acceleration was also employed to realize synchrotron radiation in both temporal [45] and spatial [64] domain.

Under a strong self-defocusing nonlinearity, a solution having sufficiently wide main lobe should exist in Eq.(2). Consequently, the diffraction/dispersion term in Eq.(2) may be safely neglected, leading to a pure nonlinear effect in the nonlinear state. Using the Thomas-Fermi approximation, one has $[hs + f(I)]\, u = 0$ that is only satisfied when $hs + f(I) = 0$. Then the following formula is reached:

$$s = -f(I)/h \tag{3}$$

where one can infer that it is possible to map a nonlinear response to a real dimension (space or time) [65].

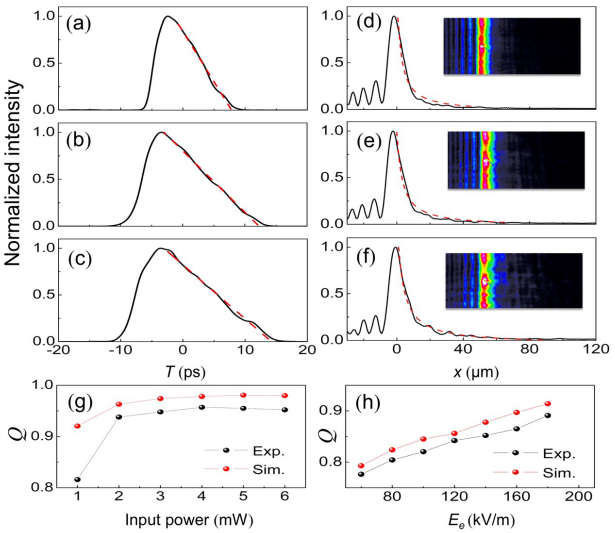

FIG. 2. Upper three rows: Nonlinear output of a modulated Airy pulse (left) and beam (right) experiencing the Kerr and the photorefractive self-defocusing nonlinearity that is strengthened from top to bottom, respectively. T (or x) is the time delay (or transverse coordinate). The beam profiles in (d-f) are obtained by integrating the captured output beam patterns in the corresponding insets. The dashed red lines are used for fitting the right sides of the main lobes. (g) and (h) show the similarity between the fitting data and the target nonlinear response functions.

To verify this prediction, an experiment is performed in a 3.9-km nonlinear optical fiber to test the Kerr-type nonlinearity. The probe pulse is positioned in the normal dispersion region to gain a self-defocusing nonlinearity. As mentioned at the beginning of this Section, it is possible to approach the nonlinear mode via the adiabatic evolution of a modulated Airy field. To this end, in the linear case, an Airy pulse is delivered to the fiber output by employing a quadratic phase. Under the action of the self-defocusing nonlinearity, the output pulse shows a broadening as the input power is turned up [Figs. 2(a-c)]. As expected, their trailing edges are fitted well with the Kerr response function. Next, the mapping experiment is also performed in the spatial domain for a photorefractive nonlinearity offered by a photorefractive crystal (SBN: 61 with dimensions $5 \times 5 \times 10$ mm^3). The associated response function is expressed by $f(I) = -0.5n^3\gamma_{33}E_e/(1+I)$, where n is the unperturbed refractive index, γ_{33} is the electro-optic coefficient for the extraordinarily polarized beams, and E_e is the external bias field. The probe Airy beam is generated by using a properly titled cylin-

drical lens [66], having an Airy shape horizontally yet keeping quasi-invariant vertically. Before the nonlinear test, the crystal is adjusted to allow the peak intensity of the Airy beam to appear at the exiting face for the purpose of the adiabatic evolution. As the bias field increases, the main lobe of the output exhibits a broadening effect, yet in a scenario different from the Kerr case. By using Eq. (3) to fit the right side of the beam profile, the good fitting indicates that the photorefractive nonlinear response is also mapped to the nonlinear output [Figs. 2(d-f)].

To characterize the similarity between the experimental curves and the corresponding target response function, a parameter Q defined as $Q = 1 - \sqrt{\Sigma(F-I)^2/\Sigma F^2}$ is used, where F describes the fitting values. Note that lager Q indicates a higher similarity and $Q = 1$ reflects an exact overlapping. The associated calculations are summarized in Figs. 2(g) and 2(h). For the Kerr case, the value of Q is positively proportional to the strength of the nonlinearity until the input power is turned up to 4 mW where a saturation starts [Fig. 2(g)]. For the photorefractive case, Q keeps going up with the bias field yet does not reach a saturable level in the range of applied voltages [Fig. 2(h)]. Additional simulations show that the saturation is possible for further increasing the voltage, but in experiment, it is better to avoid this test due to a possible depolarization of the crystal.

The above theory and experiments both indicate that the nonlinear response function can be visualized by using a probe of a modulated Airy field. Up to now, only the case of self-defocusing nonlinearity is discussed. It is also possible to visualize a nonlinear term in a physical system that originally leads to self-focusing nonlinear dynamics. This can be achieved by reversing the sign of the associated dispersion/diffraction to satisfy the condition of an equivalent self-defocusing evolution.

IV. LIGHT-BY-LIGHT CONTROL

The implementation of the Airy beams/pulses for controlling signals has shown its infancy in recent years. In spatial domain, the Airy beams are good candidates for all-optical routing technique and all-optical interconnections [10,11]. In the temporal case, it is shown that the Airy pulse can be used to control a soliton via an event horizon [67]. In much earlier works, Raman solitons were employed to trap and guide signals, relying on its decelerating manner, but their acceleration is difficult to control [68,69]. Alternatively, the Airy pulses, featured with a reconfigurable acceleration, have the ability to realize such steering functions in a more controllable way [70,71].

To have a better understanding on the pulse-by-pulse control, simulations are performed by using the following equations:

$$i\frac{\partial A}{\partial z} = \frac{\beta_{2A}}{2}\frac{\partial^2 A}{\partial T^2} + i\frac{\beta_{3A}}{6}\frac{\partial^3 A}{\partial T^3} - \gamma_A|A|^2 A \qquad (4a)$$

$$i\frac{\partial B}{\partial z} = \frac{\beta_{2B}}{2}\frac{\partial^2 B}{\partial T^2} + i\frac{\beta_{3B}}{6}\frac{\partial^3 B}{\partial T^3} - 2\gamma_B|A|^2 B \qquad (4b)$$

where A and B are the envelopes of an Airy and a signal pulse, respectively, z is the propagation distance in lab frame, β_{2A} and β_{2B} (β_{3A} and β_{3A}) are the coefficients of the second-order (third-order) dispersion, and $\gamma_A = \gamma_B = \gamma$ are the nonlinear coefficients. Mild input power is injected for the Airy pulse to keep its acceleration in the self-focusing nonlinear propagation, while the signal pulse having a quite low power does not feel any nonlinearity. The two pulses co-propagate in a fiber. Figures 3(a-c) display the evolution of the signal with different time delays to the Airy pulse whose main peak is traced out by the white dash lines. For near zero time delay, the signal pulse can be almost totally trapped and guided [Fig. 3(a)]; while for the other cases, only part of the signal is forced to co-accelerate with the Airy pulse [Figs. 3(b) and (c)]. These dynamics are clearly revealed in the measured spectra of the signal [Fig. 3(d)]. A significant red-shift wavelength conversion is realized for the signal having near zero time delay to the Airy pulse. In the same vein, a blue shift is also reached by reversing the acceleration sign of the Airy pulse [Fig. 3(e)]. Furthermore, such wavelength conversion can be tuned by changing the acceleration strength of the Airy pulse. Via decreasing the modulation depth defined by a (corresponding to the increase of the acceleration) while keeping near-zero time delay of the two pulses, the signal is transferred to a shorter wavelength [Fig. 3(f)].

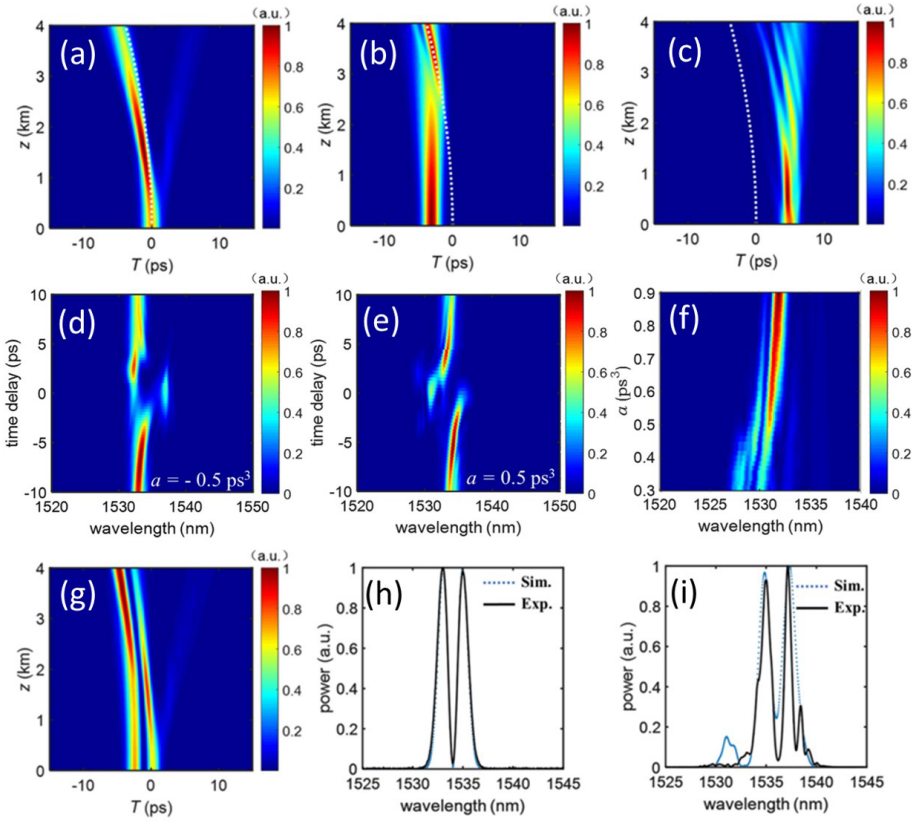

FIG. 3. (a-c) Simulated propagation of a single-peak signal pulse co-propagating with an Airy pulse (whose main lobe is traced out by the white dotted lines) for different initial time delays of the two pulses. (d-f) Measured output spectra of the signal with different initial time delays to the Airy pulses that have opposite acceleration signs (d,e), or with near-zero time delay yet using different values of the acceleration (f). (g) Simulated guiding and routing of a double-peak signal. (h) and (i) show the input and output spectra obtained from the simulation/experiment corresponding to (g), respectively.

Inspired by the fact that a conventional (straight) spatial waveguide can support higher-order as well as fundamental modes, the accelerating potential is expected to trap and guide multi-peak signals. For the same nonlinear Airy pulse, a double-peak signal of such dynamics is found numerically [Fig. 3(g)]. In experiment, a signal having the spectral shape [Fig. 3(h)] associated with the numerical input is launched. At the output, it exhibits a red shift after a 4-km evolution in the presence of the Airy pulse, while still preserves its double-peak feature [Fig. 3(i)], attributing to the guiding effect of the accelerating potential. Additional simulations show that a much higher order mode such as three-peak signal cannot be supported, since the index change induced by the Airy pulse is not quite high under a mild nonlinearity. The mechanism of this guidance is similar to the cases by means of Raman solitons [72,73].

Apart from the aforementioned steering function, nonlinear interactions involving accelerating beams indeed have led to many novel dynamics. Airy fields were also utilized to manipulate solitons in different nonlinear environments [67,74,75]. Soliton pairs were routinely generated for the interaction of two (or more) Airy beams in strong self-focusing regime. The emitting solitons exhibit attraction and repulsion for in-phase and out-of-phase of the Airy inputs, respectively [76−79], while always show attractive behavior for mutually incoherent Airy beams [80]. The spatiotemporal dynamics of two incoherent counterpropagating Airy beams are proved to be different from the cases associated with Gaussian beams [81,82]. In addition, Airy breathers can be observed and remain robust even under a strong nonlinear condition [83−85]. In the case of nonlocal nonlinearities, one can emulate gravitational phenomenon by studying the evolution

of a broad accelerating wave packet interacting with an intense Gaussian beam. This system is analogous to the Newton – Schrödinger one, simulating gravity in the Newtonian limit together with quantum mechanics [86]. In photorefractive crystals, the possibility of optical waveguiding via the Airy beams has been discussed in both symmetric and anti-symmetric configurations [11,87]. Quite recently, pattern-forming dynamics were investigated by injecting 2D Airy beams into a nonlinear single feedback setup where two-wave mixing and modulation instability were involved. The self-organization was accompanied by a natural drifting process related to the intrinsic acceleration of the Airy beam, and the drifting dynamics can be controlled by the parameters of the Airy beam itself [88].

V. OPTICAL DIAMETRIC DRIVE ACCELERATION

For the Airy-like nonlinear accelerating optical fields, only the most intense part exhibits an acceleration, but the overall profile still evolves along a straight line. One may wonder whether the beam/pulse can be designed to show a full acceleration. Such optical dynamics become real by introducing the concept of runaway motion [89], where matters having opposite mass signs show a joint acceleration during their interaction. This intriguing behavior originates from the non-intuitive effect brought by negative mass. The action-reaction symmetry, governed by Newton's third law, is broken in such a captivating motion. In optics, the pulses experiencing dispersion of opposite signs show the analogous dynamic behavior for the objects of opposite mass signs. During their nonlinear interaction in fibers, they are bounded to accelerate in the same direction [90,91], namely optical diametric drive acceleration. Quite recently, this intriguing interaction was also realized in the spatial domain, by employing optical beams experiencing normal and anomalous diffractions of an optical lattice in analog to objects of opposite mass signs [92–94]. The reciprocal property of interactions can be also broken by presetting the associated forces to be the same direction in liquid crystals [95]. It is worth noting that, other than a diametric drive acceleration, the interaction between solitons having effective mass of opposite signs allows for shuttle motions and splitting when the nonlinearity and mass are carefully tuned in Bose-Einstein condensates [96].

By means of the optical coherence, such diametric drive acceleration was readily extended into the coherent regime [93,94], showing exotic features non-existed in the classic case. The associated study was performed in a one dimensional (1D) optical lattice fabricated by titanium in-diffusion in a nonlinear photorefractive $LiNbO_3$ crystal. The beam propagation in this optical structure is governed by the paraxial nonlinear Schrödinger equation:

$$i\frac{\partial\varphi}{\partial z}+\frac{1}{2nk_0}\frac{\partial^2\varphi}{\partial x^2}+k_0C\cos^2(\pi x/\Lambda)\varphi=\Gamma\frac{|\varphi|^2}{1+|\varphi|^2}\varphi \quad (5)$$

where φ is the slowly varying complex amplitude of an incident beam, x (or z) is the transverse (or longitudinal) coordinate, k_0 is the wave number in the vacuum, and n is the unperturbed refractive index of the crystal. The periodic potential associated with the photonic lattice is approximately modeled by a $\cos^2$ function with C being the lattice modulation depth and Λ being the lattice constant. The nonlinear coefficient is $\Gamma = k_0 n\gamma_{33}E_{\rm pv}/2$, where γ_{33} is the electro-optical coefficient, and $E_{\rm pv}$ is the photovoltaic field. Figure 4(a) shows a schematic diffraction relationship of a 1D optical lattice in the first Brillouin zone (BZ). The diffractions at the top (Γ point) and the bottom (M point) edges exhibit opposite signs. The beams exciting the two points are named as Γ-beam and M-beam. Their experimental intensity patterns are displayed in Fig. 4(b). As presented in Ref. [92], Γ- and M-beams show inverted behaviors when encountering a negative index change embedded in a uniform lattice. The former tends to be repelled while the latter tends to be attracted. Under the action of the self-defocusing nonlinearity arising from the bulk photovoltaic effect, both Γ- and M-beams induce negative refractive index changes. When the two beams propagate together with a proper spacing, they can shift to the same transverse direction due to the symmetry breaking of action-reaction. If the initial condition is elaborately chosen, the two beams are able to bind to accelerate together. Experiments are operated in a 1.4-cm-long sample. The two mutually coherent beams with a proper spacing are launched simultaneously into the waveguide array with an equal

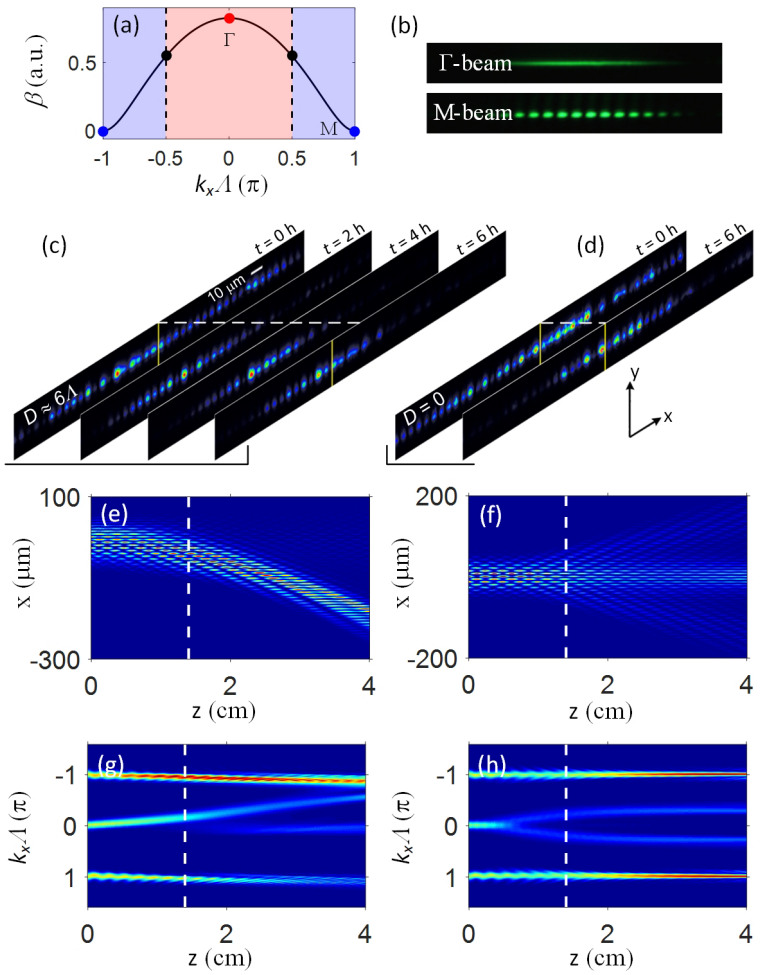

FIG. 4. Typical first Bloch band of 1D photonic lattices, where the normal and anomalous diffraction regions separated by zero-diffraction points (black), are shaded in red and blue. (b) Measured Γ- and M-beams at the input. (c,d) Temporal evolution of the output beam under the action of the nonlinearity when the initial spacing (D) between the two input beams is about six times of the lattice constant (c) and zero (d), respectively, where the yellow lines mark the "center of mass". (e,f) show the numerical simulations of the beam propagations in a steady state corresponding to (c,d), respectively. (g,h) Spatial spectral evolution corresponding to (e,f). The dashed white lines in (e-h) mark the output location of the sample.

phase. Taking the advantage of noninstantaneous photorefractive response, the temporal evolutions of the beams exiting the lattice are recorded. As summarized in Fig. 4(c), the combined output evolves from a widely spread distribution to a somewhat localized pattern, meanwhile the overall beam center (defined as $\int x\mathrm{d}x \int I\mathrm{d}y / \int\int I\mathrm{d}x\mathrm{d}y$, where I is the light intensity) at the steady-state moves along -x direction. The localization is attributed to a discrete self-trapping, while the lateral movement of the whole beam is caused by that its two components with opposite diffraction signs break the action-reaction symmetry during interaction. For comparison, the output for the two beams having zero spacing is presented in Fig. 4(d), where the lateral shift of the beam center is almost not noticed.

Numerical beam propagations simulated by using Eq. (5) at a distance longer than the sample length are shown in Figs. 4(e) and 4(f). The combined beam experiences a clear self-accelerating effect for the case of non-zero spacing between Γ- and M-beams [Fig. 4(e)], while its pattern always remains symmetrical about $x = 0$ for the other case [Fig. 4(f)]. The momentum change of the light is accordingly revealed in the (spatial) spectrum domain, i.e., in the k_x space [Figs. 4(g) and 4(h)]. In the coherent diametric drive acceleration, both spectral components located at the center and boundary of the 1st BZ exhibit a net shift due to the self-accelerating effect.

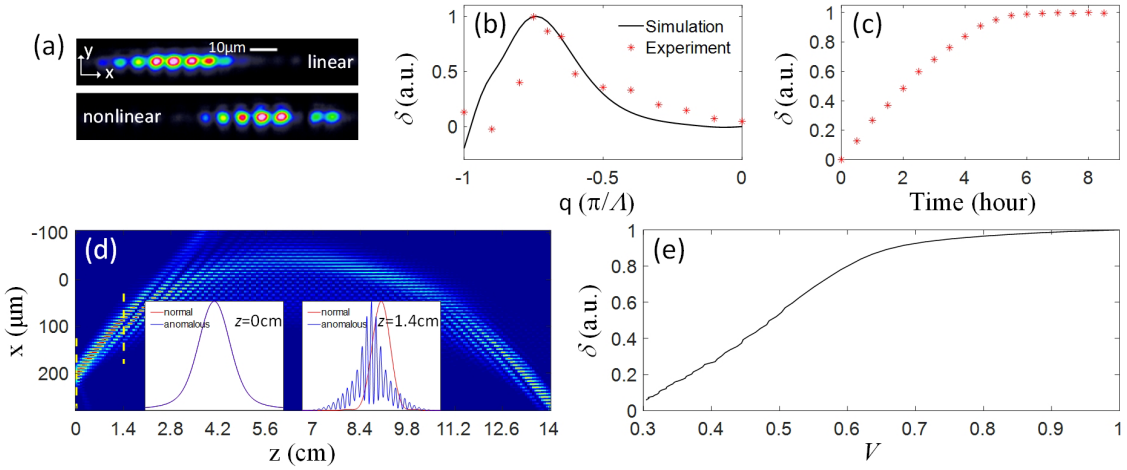

FIG. 5. (a) Measured output beams exciting the zero-diffraction point for the linear and nonlinear cases. (b,c) Beam center shifts at the output for different input tilts (b) and different evolution time (c). (d) Numerical propagation of a spontaneous diametric drive acceleration, where the insets show the beam profiles in the normal and anomalous diffraction regions at $z = 0$ and 1.4 cm. (e) Numerically calculated beam center shifts at the output for various coherence degrees.

For different phase differences initially set between the two input beams, the overall beam center changes hardly [93]. The phase insensitive behavior for the beam interactions is attributed to the beating effect of Γ- and M-beams along the waveguide array. The coherent diametric drive acceleration always shows a larger shift of the beam's central position comparing to its incoherent counterpart (where the two input beams are switched into a mutually incoherent regime [92]).

It should be noted that the normal and anomalous diffraction regions are separated by a special point named zero-diffraction point [Fig. 4(a)]. A single beam, launched near this point, should cover both diffraction regions, leading to a possibility to form the ingredients required for an optical diametric drive acceleration. Thus, the beam may show a spontaneous bending under the action of a nonlinearity [94]. Figure 5(a) shows the experimental outputs in the linear and nonlinear cases by employing a Gaussian beam to excite the zero-diffraction point. A clear transverse movement of beam is observed as the nonlinearity takes effect. The parameter δ is used to characterize the beam deflection, defined by the difference between the beam centers for the linear and nonlinear outputs. The influence of the input beam tilting on the spontaneous bending propagation is examined. The optimized value appears near the tilt exciting the zero-diffraction point, i.e., $q = -0.75\pi/\Lambda$ [Fig. 5(b)]. Furthermore, using this optimized tilt, the influence of the nonlinear strength is studied. As time flies (corresponding to strengthening the nonlinearity with the help of a photorefractive effect), the beam center shift continuously increases until a steady state is reached [Fig. 5(c)].

The mechanism behind the spontaneous bending is understood by further analyzing the real space evolution of the components experiencing different types of diffractions. Initially, the two components overlap exactly. During the nonlinear interaction, they fail to occupy the same location. Specifically, under the self-defocusing nonlinearity, the negative index change induced by the component in the anomalous (normal) diffraction region is able to repel (attract) the part experiencing the normal (anomalous) diffraction. The part in the normal diffraction region prefers to stay at only one side [here right side as shown in the inset of Fig. 5(d)] of the other part, since its self-defocusing evolution is asymmetric near the zero-diffraction point where the maximum beam tilt in the photonic lattice is defined. Consequently, they constitute a pair similar to that in a coherent diametric drive acceleration [93] and move jointly in a self-accelerating manner during the following propagation. Finally, the incoherence is taken into account for studying the spontaneous effect. The visibility V is employed to characterize the coherence of the input beam. Larger value of V corresponds to a higher degree of coherence. Simulations presented

in Fig. 5(e) show that the beam center shift decreases as the coherence is reduced, indicating a weaker diametric drive acceleration. But for a mild incoherence degree (say, $V > 0.6$), the accelerating strength is still considerable.

VI. CONCLUSION

In this short review, we have briefly discussed the nonlinear self-accelerating wave packets and their applications. They brought about exotic features by shaping the nonlinear processes into an accelerating manner, and along this line, various appealing applications were put forward. Recently, a new kind of self-accelerating wave packets based on a runaway mechanism was demonstrated, allowing for more possibilities to study nonlinear dynamics in a curved space or spacetime. Comparing to the numerous investigations on the nonlinear dynamics of Airy wave packets focusing on their field structures, the acceleration property of self-accelerating wave packets is still much less explored. As the unique property for these beams/pulses, the acceleration may bring about more unexpected nonlinear phenomena and effects that do not exist for the case of a straightly moving intense peak. So far, the accelerating nonlinear process has been mainly studied in a 2D configuration including one evolution dimension and one space or time. Extending to higher dimensions, more novel dynamics will be expected with the blooming of intriguing optical fields in common with the Airy wave packets.

REFERENCES

[1] Berry M V, Balazs N L. *Am. J. Phys.*, 1979, **47**: 264
[2] Siviloglou G A, Christodoulides D N. *Opt. Lett.*, 2007, **32**: 979
[3] Siviloglou G A, Broky J, Dogariu A, Christodoulides D N. *Phys. Rev. Lett.*, 2007, **99**: 213901
[4] Baumgartl J, Mazilu M, Dholakia K. *Nat. Photon.*, 2008, **2**: 675
[5] Baumgartl J, Hannappel G M, Stevenson D J, Day D, Gu M, Dholakia K. *Lab on a chip*, 2009, **9**: 1334
[6] Jia S, Vaughan J C, Zhuang X. *Nat. Photon.*, 2014, **8**: 302
[7] Vettenburg T, Dalgarno H I, Nylk J, *et al. Nat. Methods*, 2014, **11**: 541
[8] Wang J, Hua X, Guo C, *et al. Optica*, 2020, **7**: 790
[9] Mathis A, Courvoisier F, Froehly L, *et al. Appl. Phys. Lett.*, 2012, **101**: 071110
[10] Rose P, Diebel F, Boguslawski M, Denz C. *et al. Appl. Phys. Lett.*, 2013, **102**: 101101
[11] Wiersma N, Marsal N, Sciamanna M, Wolfersberger D. *Opt. Lett.*, 2014, **39**: 5997
[12] Liang Y, Hu Y, Song D, *et al. Opt. Lett.*, 2015, **40**: 5686
[13] Abdollahpour D, Suntsov S, Papazoglou D G, Tzortzakis S. *Phys. Rev. Lett.*, 2010, **105**: 253901
[14] Chong A, Renninger W H, Christodoulides D N, Wise F W. *Nat. Photon.*, 2010, **4**: 103
[15] Hu Y, Siviloglou G A, Zhang P, Efremidis N K, Christodoulides D N, Chen Z. *Self-accelerating Airy Beams: Generation, Control, and Applications*, in Nonlinear photonics and novel optical phenomena, Z. Chen and R. Morandotti, eds, (Springer, 2012) 170, 1
[16] Zhang Y, Zhong H, Belić M, Zhang Y. *Appl. Sci.*, 2017, **7**: 341
[17] Efremidis N K, Chen Z, Segev M, Christodoulides D N. *Optica*, 2019, **6**: 686
[18] Polynkin P, Kolesik M, Moloney J. *Phys. Rev. Lett.*, 2009, **103**: 123902
[19] Polynkin P, Kolesik M, Moloney J V, Siviloglou G A, Christodoulides D N. **Science**, 2009, **324**: 229
[20] Clerici M, Hu Y, Lassonde P, *et al. Sci. Adv.*, 2015, **1**: e1400111
[21] Chen R P, Yin C F, Chu X X, Wang H. *Phys. Rev. A*, 2010, **82**: 043832
[22] Jia S, Lee J, Fleischer J W, *et al. Phys. Rev. Lett.*, 2010, **104**: 253904
[23] Hu Y, Huang S, Zhang P, *et al. Opt. Lett.*, 2010, **35**: 3952
[24] Dolev I, Kaminer I, Shapira A, *et al. Phys. Rev. Lett.*, 2012, **108**: 113903
[25] Dolev I, Libster A, Arie A. *Appl. Phys. Lett.*, 2012, **101**: 101109
[26] Allayarov I M, Tsoy E N. *Phys. Rev. A*, 2014, **90**: 023852
[27] Zhou G, Chen R, Ru G. *Laser Phys. Lett.*, 2014, **11** 105001
[28] Mayteevarunyoo T, Malomed B A. *Opt. Lett.*, 2015, **40**: 4947
[29] Kong Q, Wei N, Fan C, Shi J, Shen M. *et al. Sci. Rep.*, 2017, **7**: 4198
[30] Kong Q, Wei N, Fan C, Shi J, Shen M. *Sci. Rep.*, 2017, **7**: 4198
[31] Liang X, Zhang Z, Li D, Han X, Gao F, Chen Z. *Opt. Commun.*, 2019, **437**: 90
[32] Hu Y, Li M, Bongiovanni D, *et al. Opt. Lett.*, 2013, **38**: 380 (2013)
[33] Driben R, Hu Y, Chen Z, *et al. Opt. Lett.*, 2013, **38**: 2499
[34] Zhang L, Zhang J, Chen Y, *et al. J. Opt. Soc. Am. B*, 2014, **31**: 889
[35] Zhang L, Zhong H. *Opt. Express*, 2014, **22**: 17107
[36] Zhang L, Zhong J, Li Y, Fan D. *et al. Opt. Express*, 2014, **22**: 22598
[37] Zhang L, Liu K, Zhong H, *et al. Sci. Rep.*, 2015, **5**: 11843
[38] Zhang L, Liu K, Zhong H, *et al. Opt. Express*, 2015, **23**: 2566
[39] Zhang L, Liu K, Zhong H, *et al. J. Opt.*, 2016, **18**: 015505

[40] Deng F, Hong W, Deng D. *Opt. Express*, 2016, **24**: 15997
[41] Yu Y, Zhang Y, Song X, *et al. IEEE Photon. J.*, 2017, **9**: 1
[42] Yan X, Zhang X, Liu F, *et al. IEEE Photon. J.*, 2017, **9**: 3
[43] Zhang L, Huang P, Conti C, *et al. Opt. Express*, 2017, **25**: 1856
[44] Hu Y, Li Z, Wetzel B, *et al. Sci. Rep.*, 2017, **7**: 8695
[45] Zhang L, Zhang X, Pierangeli D, *et al. Opt. Express*, 2018, **26**: 14710
[46] Ament C, Polynkin P, Moloney J V. *Phys. Rev. Lett.*, **107**: 243901
[47] Hu Y, Tehranchi A, Wabnitz S, *et al. Phys. Rev. Lett.*, 2015, **114**: 073901
[48] Driben R, Meier T. *Opt. Lett.*, 2014, **39**: 5539
[49] Kaminer I, Segev M, Christodoulides D N. *Phys. Rev. Lett.*, 2011, **106**: 213903
[50] Lotti A, Faccio D, Couairon A, *et al. Phys. Rev. A*, 2011, **84**: 021807(R)
[51] Hu Y, Sun Z, Bongiovanni D, *et al. Opt. Lett.*, 2012, **37**: 3201
[52] Ruizjimenez C, Nobrega K Z, Porras M A. *Opt. Express*, 2015, **23**: 8918
[53] Bekenstein R, Segev M. *Opt. Express*, 2011, **19**: 23706
[54] Aleahmad P, Miri M A, Mills M S, *et al. Phys. Rev. Lett.*, 2012, **109**: 203902
[55] Courvoisier F, Mathis A, Froehly L, *et al. Opt. Lett.*, 2012, **37**: 1736
[56] Zhang P, Hu Y, Cannan D, et al. *Opt. Lett.*, 2012, **37**: 2820
[57] Kaminer I, Nemirovsky J, Segev M. *Opt. Express*, 2012, **20**: 18827
[58] Schley R, Kaminer I, Greenfield E, *et al. Nat. Commun.*, 2014, **5**: 5189
[59] Qi X, Makris K G, El-Ganainy R, *et al. Opt. Lett.*, 2014, **39**: 1065
[60] Makris K G, Kaminer I, Elganainy R, *et al. Opt. Lett.*, 2014, **39**: 2129
[61] Fattal Y, Rudnick A, Marom D M. *Opt. Express*, 2011, **19**: 17298
[62] Wiersma N, Marsal N, Sciamanna M, Wolfersberger D. *Sci. Rep.*, 2016, **6**: 35078
[63] Bouchet T, Marsal N, Sciamanna M, Wolfersberger D. *Phys. Rev. A*, 2018, **97**: 051801(R)
[64] Henstridge M, Pfeiffer C, Wang D, *et al. Science*, 2018, **362**: 439
[65] Jia P, Li Z, Hu Y, *et al. Phys. Rev. Lett.*, 2019, **123**: 234101
[66] Papazoglou D G, Suntsov S, Abdollahpour D, Tzortzakis S. *Phy. Rev. A*, 2010, **81**: 061807(R)
[67] Cai W, Mills M S, Christodoulides D N, Wen S. *Opt. Commun.*, 2014, **316**: 127
[68] Gorbach A V, Skryabin D V. *Nat. Photon.*, 2007, **1**: 653
[69] Liu C, Rees E J, Laurila T, *et al. Opt. Express*, 2012, **20**: 6316
[70] Goutsoulas M, Paltoglou V, Efremidis N K. *J. Opt.*, 2017, **19**: 115505
[71] Li Z, Zhang P, Mu X, *et al. Photon. Res.*, 2019, **7**: 1087
[72] Gorbach A V, Skryabin D V. *Phys. Rev. A*, 2007, **76**: 053803
[73] Roy S, Bhadra S K, Saitoh K, *et al. Opt. Express*, 2011, **19**: 10443
[74] Rudnick A, Marom D M. *Opt. Express*, 2011, **19**: 25570
[75] Shi Z, Li H, Zhu X, Chen Z. *EPL*, 2018, **124**: 14006
[76] Zhang Y, Belic M, Wu Z, *et al. Opt. Lett.*, 2013, **38**: 4585
[77] Zhang Y, Belić M R, Zheng H, *et al. Opt. Express*, 2014, **22**: 7160
[78] Diebel F, Bokic B, Timotijevic D V, *et al. Opt. Express*, 2015, **23**: 24351
[79] Zhang M, Huo G, Zhong H, Hui Z. *Opt. Express*, 2017, **25**: 22104
[80] Shen M, Wu L, Gao M, Li W. *J. Phys. B: Atomic, Molecular and Optical Physics*, 2018, **51**: 165401
[81] Wiersma N, Marsal N, Sciamanna M, Wolfersberger D. *Sci. Rep.*, 2015, **5**: 13463
[82] Marsal N, Wiersma N, Sciamanna M, Wolfersberger D. *Sci. Rep.*, 2019, **9**: 5004
[83] Driben R, Konotop V V, Meier T. *Opt. Lett.*, 2014, **39**: 5523
[84] Shen M, Gao J, Ge L. *Sci. Rep.*, 2015, **5**: 9814
[85] Shen M, Li W, Lee R. *Opt. Express*, 2016, **24**: 8501
[86] Bekenstein R, Schley R, Mutzafi M, *et al. Nat. Phys.*, 2015, **11**: 872
[87] Bouchet T, Marsal N, Sciamanna M, Wolfersberger D. *J. Phys.: Photonics*, 2019, **1**: 025001
[88] Drouzi L, Maufay J, Sciamanna M, Wolfersberger D, Marsal N. *Opt. Lett.*, 2019, **45**: 9
[89] Bondi H. *Rev. Mod. Phys.*, 1957, **29**: 423
[90] Wimmer M, Regensburger A, Bersch C, *et al. Nat. Phys.*, 2013, **9**: 780
[91] Batz S, Peschel U. *Phys. Rev. Lett.*, 2013, **110**: 193901
[92] Pei Y, Hu Y, Lou C, *et al. Opt. Lett.*, 2018, **43**: 118
[93] Pei Y, Hu Y, Zhang P, *et al. Opt. Lett.*, 2019, **44**: 5949
[94] Pei Y, Wang Z, Hu Y, *et al. Opt. Lett.*, 2020, **45**: 3175
[95] Alberucci A, Jisha C P, Peschel U, Nolte S. *Phys. Rev. A*, 2019, **100**: 011802(R)
[96] Sakaguchi H, Malomed B A. *Phys. Rev. E*, 2019, **99**: 022216

非线性自加速光场及其应用

贾鹏博，裴雨苗，张　平，李致力，胡　毅，许京军

弱光非线性光子学教育部重点实验室，南开大学物理学院，天津 300071
南开大学泰达应用物理研究院，天津 300457

摘要：近年来，艾里光束/脉冲等光场因其独特的自加速传输特性以及在诸多应用中表现出的优势引起了人们极大的研究兴趣。但在非线性环境中，这类光场却面临失去其特殊结构以及加速特性的困境。为了解决这一问题，非线性自加速光场应运而生，使得非线性过程具有加速的特质。本文基于作者近期的工作回顾了非线性自加速光场的研究进展。首先讨论了它们的物理图像以及它们与艾里光场的联系，其次详细介绍了自加速特性在非线性调控、非线性响应函数的可视化以及光控光中的独特应用优势，最后介绍了一种新式的光场自加速行为 —— 可类比于经典力学中正负质量物质的相互作用过程。这些非线性自加速光场可让非线性动力学过程在弯曲时/空发生，能引起平坦空间无法实现的新现象与新应用。

关键词：光场调控；非线性光动力学；艾里光场；自加速